Photocatalytic performance of Ti/MMO/ZnO at degradation of levofloxacin: Effect of pH and chloride anions

Lorena A. Goulart[a,b,*], Angela Moratalla[b], Marcos R. V. Lanza[a,*], Cristina Saez[b], Manuel A. Rodrigo[b]

[a] *Institute of Chemistry - São Carlos, University of São Paulo, P.O. Box 780, CEP-13560-970 São Carlos, SP, Brazil*

[b] *Department of Chemical Engineering, Universidad de Castilla-La Mancha, Campus Universitario s/n, 13071, Ciudad Real, Spain*

* Corresponding author

marcoslanza@iqsc.usp.br (Marcos Roberto de Vasconcelos Lanza)

lorenaathie@hotmail.com (Lorena Athie Goulart)

Graphical Abstract

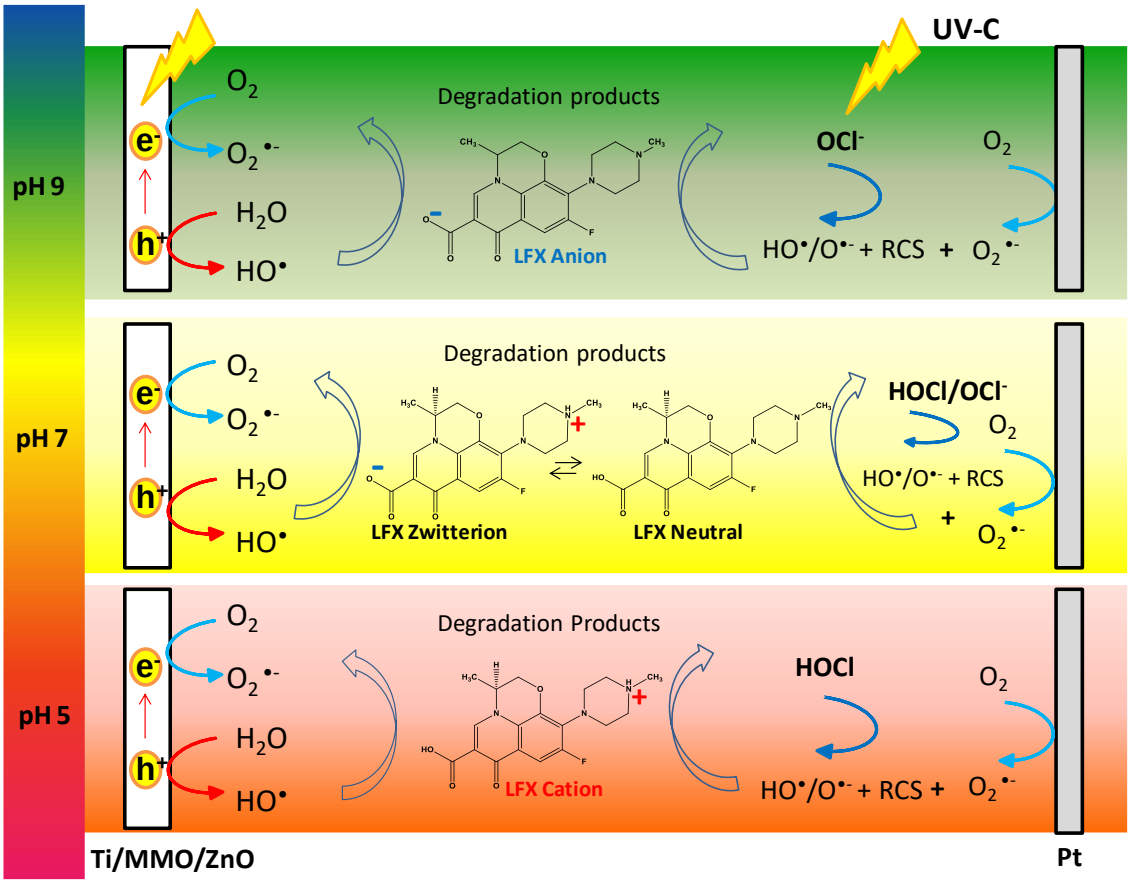

Abstract

This work investigates the applicability of a new Ti/MMO/ZnO electrode composed to metallic mixture oxides of ruthenium and titanium (MMO) and zinc oxide electrodeposited in the photoelectrocatalytic treatment of synthetic wastes polluted with the antibiotic levofloxacin (LFX) and chlorine anions. This work try to shed light, at a low Technology Readiness Level (TRL), of the mechanisms which may be involved in the degradation of antibiotics in real wastes containing high concentrations of chlorides, such as urine, in the absence of other disturbing inputs. Results show that the degradation efficiency depended on the pH of the waste and a more pronounced synergistic effect between Ti/MMO/ZnO and UVC light was obtained at acidic and

neutral pH, leading to higher rates of antibiotic removal with the subsequent formation of inorganic ions NH_4^+ and NO_3^-. The large formation of hydroxyl radicals from the photo-generated charges in Ti/MMO/ZnO, and the reactive chlorine species produced from the homolysis of hypochlorous acid/hypochlorite, are used to explain the oxidation mechanism. In addition, results indicate that Ti/MMO/ZnO is an excellent photocatalyst for the degradation under acidic conditions in wastes containing chloride anions of persistent pollutants at relatively low concentrations.

Keywords

Photoelectrolysis; Reactive chlorine species, UV-irradiation; EAOP; MMO; ZnO; levofloxacin

Highlights

- High synergism was achieved with Ti/MMO/ZnO and UVC light in the degradation of LFX

- Hydroxyl radicals, activated chlorine and charges photo-generated explain the degradation rates

- The acid-base equilibrium of LFX species influences on removal efficiency

- Photoelectrolysis has better performance at LFX removal that photolysis and electrolysis

1. Introduction

The large variety of persistent harmful pollutants found in the environment has focused the interest of the research community in recent years [1–3]. Pharmaceutical products are one of the most interesting and representative examples, with thousands of compounds that have already been detected in natural aquatic environment up to the order of µg / L [4]. The occurrence of these substances in the environment is associated to their consumption by humans and animals for the treatment of various diseases and to the low efficiency of conventional wastewater treatment plants in their removal [5,6]. Although most of the pharmaceuticals exhibit harmful characteristics, the presence of antibiotics in the water has been highlighted, because they can not only damage living ecosystems but also they can promote bacterial resistance [7].

A very interesting representative of antibiotics is Levofloxacin (LFX), which is a fluoroquinolone antibiotic used for the treatment of a wide spectrum of bacteria. Unfortunately, its presence in the environment has been associated not only to the appearance of more antibiotic-resistant bacteria, but also adverse effects on microbial communities, harming the ecosystem and affecting the human health throughout the food chain [8,9]. LFX showed cytotoxic effects in rat cells, reducing cell viability in concentrations of 10 to 80 µg/mL [10]. In addition, it presented phytotoxicity in yellow lupine, altering the protein profile of seedlings with EC50 between 1.05 and 0.069 mM [11]. To remove antibiotics from wastewater and natural water, several technologies have been investigated in the recent years [2,12–16]. Semiconductor photocatalysis is an economical green technology that stands out due to its high efficiency in the elimination of various recalcitrant contaminants from wastewater [17,18]. However, its success is directly related to the material used as a photocatalyst, since these are generally unstable and limited by the recombination of the photogenerated charges and restricted spectral response [19,20]. ZnO has been used as a photocatalyst due to its high photoactivity, low cost and low toxicity. However, different strategies have been

studied to improve the photostability of ZnO, since this oxide can undergo photo-corrosion under the incidence of continuous light. Among these strategies, the doping of ZnO with other semiconductor oxides or metals and the immobilization of this oxide on metallic mixture oxides (MMO) have achieved promising results [21–23]. Thus, the Ti/MMO/ZnO electrode could be a promising photoanode for the treatment of recalcitrant organic compounds according to its high stability, photoactivity and easy sinthesis when compared to some photoanodes previously reported in the literature [24–26].

In addition to photocatalysis, other advanced oxidative processes (AOPs) have demonstrated to be able to reach high efficiencies in the degradation of micropollutants. The key for a successful operation of AOPs is the promotion in the production or powerful radicals like the hydroxyl radicals (HO•). However, these processes are not only based on the production of HO• but also of sulfate radicals ($SO_4^{\bullet -}$) and/or reactive chlorine species (RCS). Trying to enhance the efficiency, one of the most interesting strategies to obtain radicals consists of the irradiation of ultraviolet (UV) light during treatment [27]. Presence of chlorides can promote the formation of HO• and of many RCS, with a positive effect on the removal efficiency. However, RCS can also lead to the formation of toxic by-products such as chlorite (ClO_2^-), chlorate (ClO_3^-) and perchlorate (ClO_4^-) ions [28,29]. Another disadvantage of using solutions with chlorides is their toxicity to certain freshwater species (LC50s from 682 to 1,941 mg Cl^-/L for some crustaceans and molluscs) [30], making it difficult to dispose of the post-treated waste. Because of that, it is convenient to evaluate more details about the treatment trying to determine if there is a positive input in the removal of recalcitrant pollutants with the formation of RCS[31].

Within this context, this work investigated the combination the electrolysis and photoelectrolysis of a synthetic solution containing chloride and LFX with a

Ti/MMO/ZnO electrode assisted by UV. This can be considered as a first approach, made at a low technology readiness level (TRL), for the understanding of the mechanisms which may be involved in the degradation of antibiotics in real wastes containing high concentrations of chlorides, such as urine, in the absence of other disturbing inputs.

2. Experimental

2.1 Chemicals

Levofloxacin (99%), ruthenium (III) chloride ($RuCl_3.xH_2O$, 99.9%), titanium (IV) butoxide (97%) and zinc acetate (99%) were from Sigma-Aldrich. Sodium chloride and potassium nitrate were purchased from Panreac. Methanol and formic acid (HPLC grade) were obtained Sigma-Aldrich. All aqueous solutions were prepared with ultrapure water from a Millipore Mili-Q Gradient system (resistivity 18.2 MΩ cm).

2.2 Ti/MMO/ZnO synthesis and characterization

Ti/MMO/ZnO was obtained by electrodeposition step followed by calcination. Firstly, the deposition of MMO on a titanium substrate (6.25 cm^2 area) was carried out by brushing a precursor solution of ruthenium chloride and titanium butoxide ($Ru_{0.3}/Ti_{0.7}$ molar ratio) and ionic liquid [32]. MMO layers were made until reaching a mass of 1.2 mg cm^{-2}. For each brushed layer, the film was heat treated for 5 min at 400 ° C (heating 5 °C min^{-1}). Upon reaching the desired mass, the MMO film was calcined at 400 °C for 1h. Then, the ZnO film was electrodeposited on the Ti/MMO substrate by applying –1.1 V in 0.1 mol L^{-1} solution of potassium nitrate containing 50 mmol L^{-1} of zinc acetate, with pH 5.8 adjusted with 2.0 mmol L^{-1} nitric acid solution. The precursor solution of ZnO was maintained at 80 °C during electrodeposition for 30 min. Then, the films were washed with purified water and calcined at 400 ° C with a heating ramp of 5 ° C min^{-1} for 1 h.

The surface morphology of the Ti/MMO/ZnO and their elementary composition were carried out employing a field emission scanning electron microscope with a coupled energy-dispersive X-ray spectroscopy analyzer (FE-SEM; Zeiss GeminiSEM 500 - EDX). X-ray diffraction patterns (XRD) measurements were obtained using a Bruker-D8 Advanced X-ray diffractometer with Cu Kα radiation over a 2θ range 20°–80°; scan rate of 0.02° min^{-1}.

2.3 Photoelectrocatalytic activity performance tests

For electrolysis of levofloxacin antibiotic, the Ti/MMO/ZnO electrode (geometric area of 6.25 cm^2) was used as an anode, Pt plate as a cathode and Ag/AgCl (saturated KCl) from Metrohm as the reference electrode. A UVC lamp (254 nm, 9 W) was used as light source in the photolysis and photoelectrolysis measurements. The degradation experiments were carried out in a single compartment electrochemical cell, with a capacity of 150 mL and with the lamp placed in the center. A 0.1 mol L^{-1} NaCl solution was used as supporting electrolyte and the Levofloxacin concentration was 20 ppm. The effect of UV light and the pH of solution on the degradation tests were evaluated. All electrochemical measurements were performed with a potentiostat/galvanostat (Autolab PGSTAT 302N - Metrohm).

2.4 Analytical techniques

Before analysis, all samples were filtered using a 0.22 µm filter. Aromatics were monitored by HPLC using an Agilent 1100, equipped with a diode matrix detector and Eclipse Plus C-18 column (4.6 mm × 100 mm; 3.5 µm). The wavelength used for the detection was set at 288 nm and the temperature at 40 ° C. The mobile phase consisted of 30% acetonitrile and 70% water with 0.1% formic acid (flow rate of 0.6 mL min^{-1} and an injection volume of 20 µL). Carboxylic acids were detected at 210 nm by HPLC with a ZorbaxSB-Aq column (4.6 mm × 150 mm) using a 5.0 mmol L^{-1} H_2SO_4 solution as the mobile phase. The concentration of total organic carbon (TOC) was measured on

a TOC analyzer from the Multi N/C 3100 Analytik Jena. Total oxidants were determined by iodometric titration according to Kolthoff & Carr [33]. Inorganic ions (Cl^-, ClO_3^-, NH_4^+ and NO_3^-) were monitored using a Metrohm 930 Compact IC Flex ion chromatograph with conductivity detector. For the anions, a mobile phase with 85% Na_2CO_3 and 15% acetone and a Metrosep A Supp 7 column were used. For the cations, it was used a Metrosep C6 250 column with a mobile phase of 1.7 mmol L^{-1} HNO_3 and 1.7 mmol L^{-1} of 2,6-pyridinedicarboxylic acid (flow of 0.9 mL min^{-1}).

3. Results and discussion

3.1 Structural and morphological characterization

Figure 1 gives details about the material used as photocatalyst. The deposit of ZnO directly on titanium are less stable than when an intermediated mixed metal oxide (MMO) layer is placed in between the titanium and the zinc oxide and, because of that, in this work we are evaluating this more complex electrode, because there are no information about its behavior in electrolytes with high content in chloride anions. Figure 1a shows the SEM image of this intermediate Ti/MMO layer, which acts as the ZnO substrate, and in which it is observed a "cracked-mud" morphology, typically formed in oxide films obtained by thermal decomposition [34]. On this Ti/MMO layer, the ZnO layer is deposited and calcined at 400 °C, being obtained the photoactive Ti/MMO/ZnO electrode used in this study. Figure 1b shows the coating of the MMO with nanoparticles of different structures and sizes of ZnO. This distribution leads to an increase in the porosity and in the surface area of the electrode which, in turn, is expected to improve its catalytic performance. The presence of oxygen, titanium and ruthenium was confirmed on the Ti/MMO electrode by EDX analysis as shown in Figure 1c. In the Ti/MMO/ZnO electrode, only oxygen and zinc were detected, showing that the Ti/MMO substrate was completely covered with ZnO.

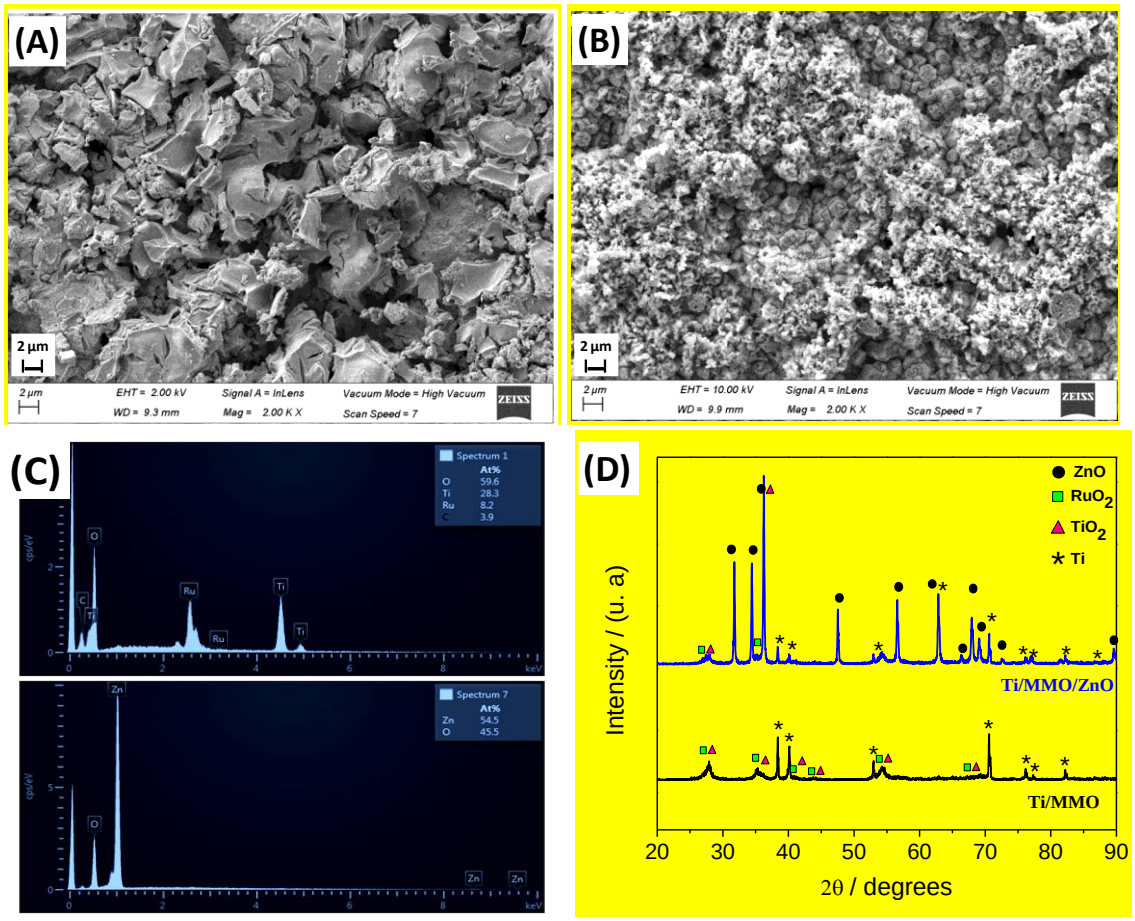

Figure 1. SEM image (A and B), EDX spectra (C) and XRD (D) of Ti/MMO and Ti/MMO/ZnO.

Crystalline structures in the Ti/MMO and Ti/MMO/ZnO were evaluated using XRD measurements (Figure 1d). In the Ti/MMO substrate, RuO_2 was formed in the rutile (JCPDS 00-040-1290), TiO_2 in the anatase (JCPDS 00-00109562) and rutile (00-004-0551) phase. In the Ti/MMO/ZnO electrode, it is remarkable the formation of ZnO with hexagonal wurtzite structure (JCPDS 36-1451). Because of the penetration of X-rays in the oxide films up to the titanium substrate, metallic Ti was also detected in the XRD [32]. Some diffraction peaks are marked with two substances (RuO_2 and TiO_2) due to the formation of a solid solution. Studies show that when obtaining mixtures of metallic oxides (MMO), solid solution and metastable structures may occur due to the high miscibility of the oxides, depending on the precursor, solvent, calcination temperature among other experimental parameters used [35,36]. Therefore, the same

diffraction peak may occur for different substances. This was also observed in other works reported in the literature in obtaining MMO composed to Ru and Ti and ionic liquid [32,37].

3.2 *Levofloxacin degradation*

Figure 2 compares changes in the LFX concentration during the photolysis, electrolysis and photoelectrolysis of a synthetic waste containing sodium chloride, sodium hydroxide (added to obtain pHs of 5.0, 7.0 and 9.0) and 20 mg L^{-1} of LFX.

The LFX degradation was very slow in the electrolysis tests and, in fact, less than 10% of the antibiotic was removed after 4 hours of treatment, regardless of the pH of the waste. LFX degradations were fitted to first order kinetic calculated by the equation: $-\ln (C / C_0) = kt$, where C_0 is the initial concentration of LFX, C is the concentration of LFX at each reaction time, t (min), and k is the reaction rate constant. From linear extrapolations shown in Figure S1 (included in supplementary materials), the rate constants were obtained. To electrolysis, the obtaining rates values were 0.016 min^{-1} (r^2 = 0.995), 0.002 min^{-1} (r^2 = 0.997) and 0.019 min^{-1} (r^2 = 0.998), respectively at the three pHs tested. The low values of the regression coefficients are related to the very low variation in the concentration of LFX during electrolysis. Opposite, in photolysis tests, the rate of degradation was much more important, and it increased with increasing the pH of the solution. After 4 hours, the degradation reached was 9.90% at pH 5, 59.7% at pH 7 and 85.3% at pH 9. Degradation results also fitted well to first order kinetics obtaining values of 0.025, 0.217 and 0.474 min^{-1}, with regression coefficients of 0.999, 0.998 and 0.998 for pHs 5.0, 7.0 and 9.0, respectively. Alkaline pHs demonstrate a very high and positive influence on the degradation of the antibiotic. The same behavior was observed in the photoelectrolysis tests, reaching degradations of LFX after 4 hours of 57.4% at pH 5.0 (0.212 min^{-1}; r^2 = 0.999), 86.8% at pH 7.0 (0.507

231 min^{-1}; r^2 = 0.998) and 97.1% pH 9.0 (0.877 min^{-1}; r^2 = 0.996). Thus, photoelectrolysis
232 was more efficient in the degradation of LFX than electrolysis or photolysis in NaCl
233 medium, showing the synergistic effect ($K_{photoelectro}$ / (K_{photo}+ $K_{electro}$))between the
234 photoactivation of Ti/MMO/ZnO by UVC light and the potential applied with values of
235 5.17, 2.31 and 1.77, respectively, at the three different pHs evaluated.

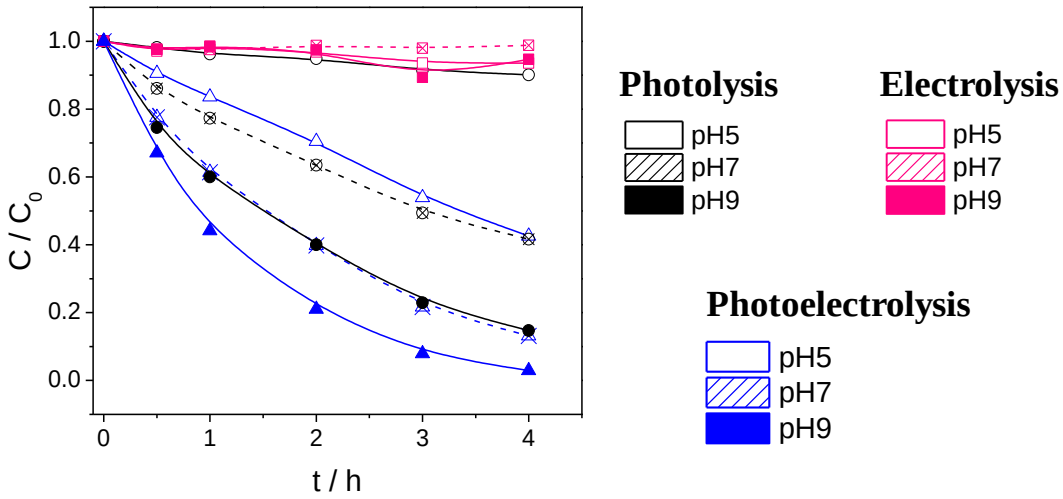

236

237 **Figure 2.** Photolysis, electrolysis (0.2 V) and photo-electrolysis (0.2V and UV) of 20
238 ppm levofloxacin with Ti/MMO/ZnO in 0.1 mol L^{-1} NaCl solutions at pH 5.0, pH 7.0
239 and pH 9.0.
240
241 Figure 3 focuses on the mineralization of the antibiotic showing the percentages
242 of TOC removal after 4 hours of treatment. The highest percentages of TOC removal
243 for electrolysis was ~ 0.11%, for photolysis ~ 13.8% and for photoelectrolysis ~ 18.0%
244 at acid and neutral pHs. Results show again the inefficiency of the bare electrolysis, the
245 unexpected good performance of photolysis and the outstanding and synergistic
246 performance of photoelectrolysis with synergistic coefficients over 1 for all pHs (3.00,
247 1.19 and 7.04 for pHs 5.0, 7.0 and 9.0, respectively). In comparing figures 2 and 3, it is
248 important to see important differences between the influence of pHs on the oxidation of
249 the LFX and the removal of TOC. Regarding mineralization, it is better to operate at
250 acidic pHs, just in the conditions in which the removal of LFX was slower. This can

only be explained in terms of the formation of higher concentrations of intermediates at neutral and alkaline pHs and, consequently, in the development of a more direct mineralization at acidic pHs, which must be associated to hasher oxidation conditions.

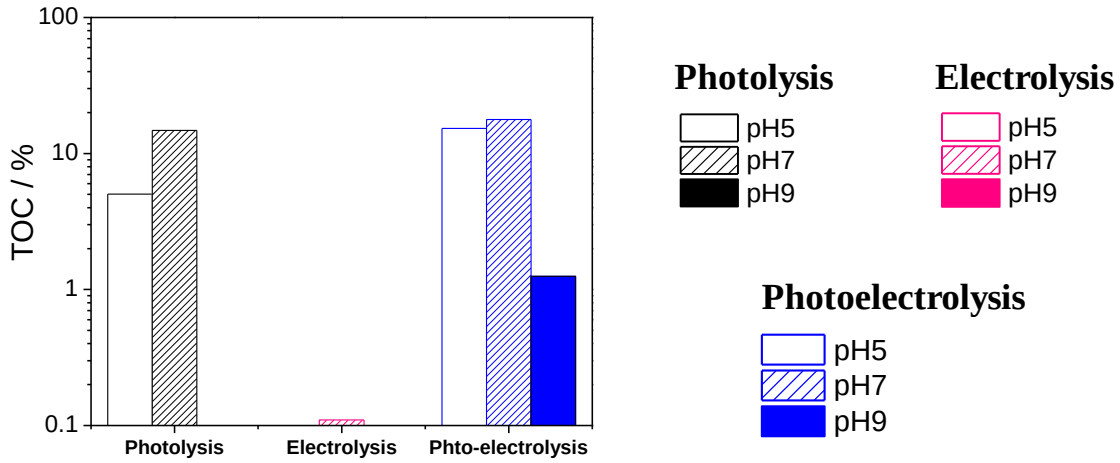

Figure 3. Removal percentage of levofloxacin at photolysis, electrolysis (0.2 V) and photo-electrolysis (0.2V and UV) with Ti/MMO/ZnO in 0.1 mol L^{-1} NaCl solutions at pH 5.0, pH 7.0 and pH 9.0.

As well, the characteristics of the LFX molecule at the different studied pHs can also affect the degradation efficiency. Levofloxacin exists as a zwitter ion and neutral species in the pH range of 6.0 to 8.0, and can undergo various acid-base equilibrium to form anionic, cationic and dipolar species with a change in pH, as shown in Figure 4 [38]. The reactivity of the ionic species of the molecule at a given pH can contribute to photodegradation. At pH close to pK_{a1} (6.02), the formation of the protonated piperazinyl group and the dissociation balance of the carboxylic acid group can influence photodegradation. At pH around pK_{a2} (8.15), partial deprotonation of the piperazinyl group occurs and at more basic pHs, the decrease in the rate of degradation may be due to the presence of the molecule in its non-protonated form [39].

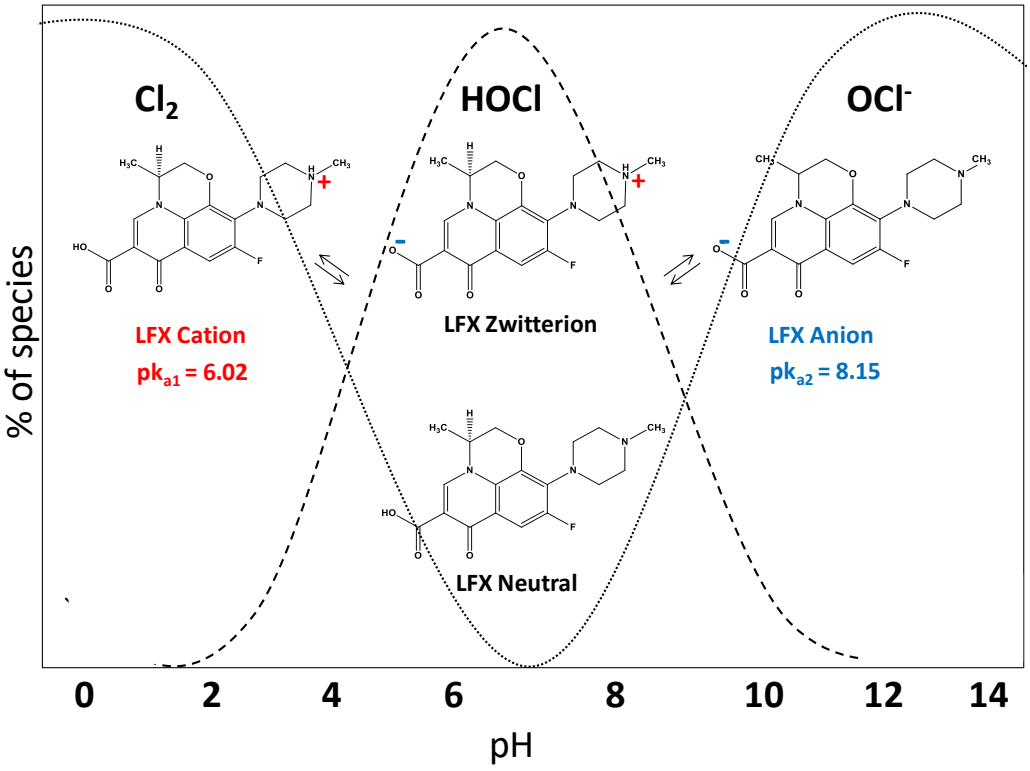

Figure 4. Speciation pattern of levofloxacin and reactive chlorine species at different pHs [38,40].

Figure 5 shows the changes in the concentrations of the aromatic intermediates formed in the LFX electrolysis, photolysis and photoelectrolysis tests (measured as chromatographic area). No intermediates were found in the electrolysis. The intermediate with a retention time of 1.7 min was detected at all studied pHs. However, at pH 9, more intermediates were formed and, consequently, detected in the retention times of 2.0 min for photolysis and photoelectrolysis; and in 4.4 min and 5.0 min for photoelectrolysis. The formation of more organic intermediates at basic pH during photolysis and photoelectrolysis agrees with the high rate of degradation of LFX molecule and the low rate of mineralization in this reaction medium.

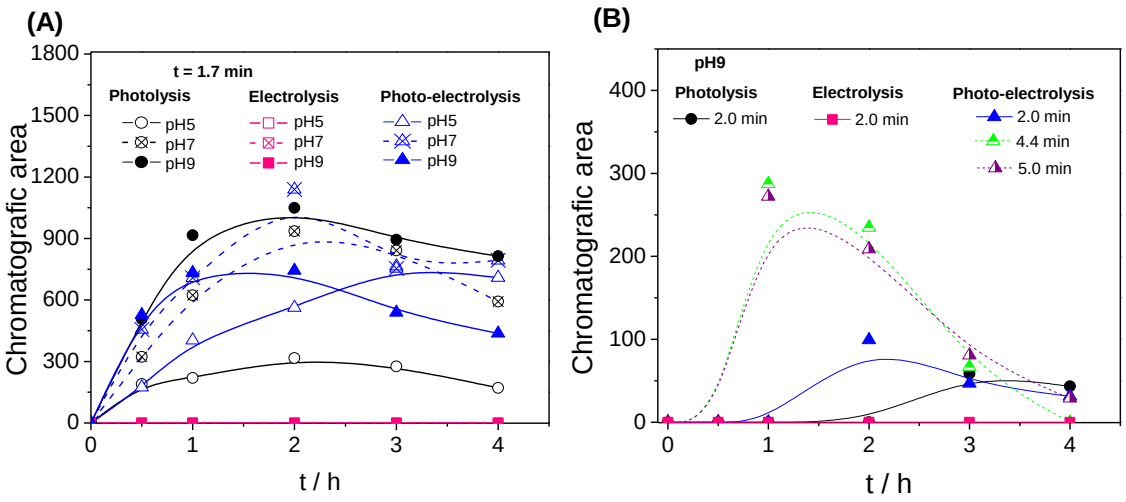

Figure 5. Intermediates formed in the experiments of photolysis, electrolysis (0.2V) and photo-electrolysis (0.2V and UV) of 20 ppm levofloxacin with Ti/MMO/ZnO in 0.1 mol L^{-1} NaCl solutions at pH 5.0, pH 7.0 and pH 9.0 (A) and pH 9.0 (B).

A similar behavior was observed in the formation of short chain acids. Oxalic, oxamic and maleic acids were formed mainly in the photoelectrolysis experiments and in neutral and basic pH, as shown in Figure 6. As for the aromatics, at these pHs, the higher increase in the concentration of acids is explained in terms of the lower mineralization reached for LFX as compared to the oxidation carried out at acidic conditions. This means that photolysis and photoelectrolysis are not promoted at neutral or alkaline pHs, leading to the accumulation of intermediates, being particularly important the increase in the concentration of carboxylic acids

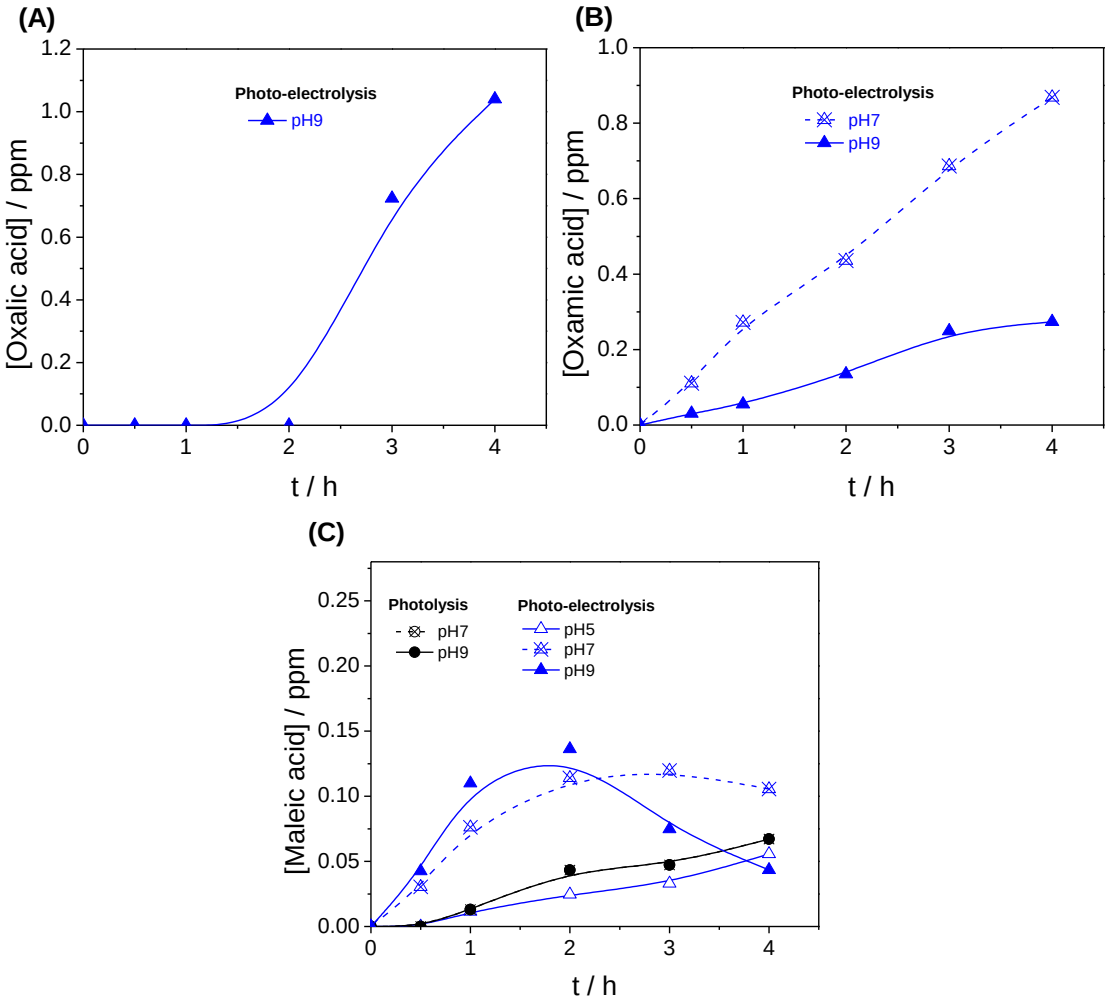

294

295

296 **Figure 6.** Carboxylic acids formed in the experiments of photolysis and photo-
297 electrolysis (0.2V and UV) of 20 ppm levofloxacin with Ti/MMO/ZnO in 0.1 mol L^{-1}
298 NaCl at pH 5.0, pH 7.0 and pH 9.0.

299 The oxidants formed during the LFX degradation in the different processes
300 studied were also monitored and are shown in Figure 7. It is important to note that the
301 oxidants measured are not the total oxidants produced at the different systems studied,
302 but those remnants that have not chemically reacted with other components of the
303 solution. This means that very reactive oxidants are not included in this value, because
304 they are expecting to act before being detected.

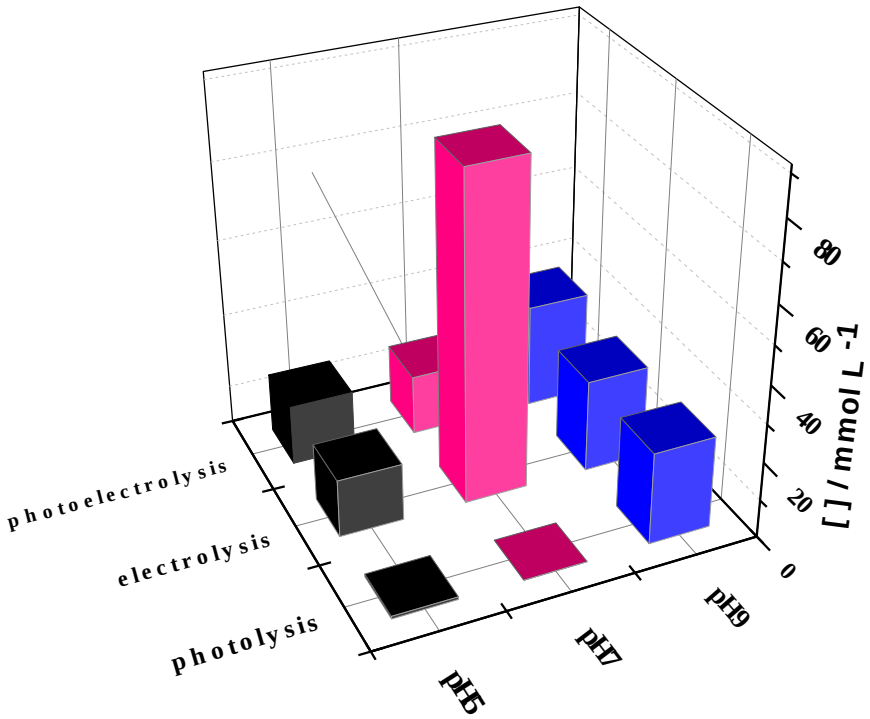

305

306 **Figure 7.** Oxidants formed in the experiments of photolysis and photo-electrolysis
307 (0.2V and UV) of 20 ppm levofloxacin with Ti/MMO/ZnO in 0.1 mol L^{-1} NaCl at pH
308 5.0, pH 7.0 and pH 9.0.

309 The concentration of oxidants varied according to the pH of the solution and the
310 oxidation processes studied. In electrolysis, higher concentrations of oxidants were
311 observed as compared to photolysis and photoelectrolysis. This higher concentration of
312 oxidants at the electrochemical process indicates that most of the oxidants produced
313 were not consumed during LFX degradation, mainly at neutral pH. This result is in line
314 with the low rate of degradation observed for LFX during electrolysis. However, in
315 photolysis and photoelectrolysis of LFX, there was a higher consumption of oxidants at
316 pH 5 and pH 7 as compared to pH 9. These results agree with the increase in the
317 removal of LFX in acidic and neutral media. Activation of oxidants with the
318 decomposition of the molecular oxidants up to short life-time radicals can help to
319 understand this behavior as the action of these later radical oxidants is known to be
320 much more intense. This decomposition is promoted with the irradiation of light and

this explains the very improved results obtained by the photoelectrolysis. At basic pH, the ease of forming hydroxyl radicals, in addition to some reactive chlorine species, may have had an antagonistic effect on the degradation of LFX due to the high concentration of these reactive species, which can recombine and finally lead to the dissipation of the oxidation power with the formation of low oxidation capacity species such as oxygen. Thus combination of hydroxyl radicals can lead to the formation of hydrogen peroxide or oxygen and combination of chlorine radicals can lead to the formation of non-desired species such as chlorates or even perchlorates [41].

Thus, in chloride solution, the degradation of levofloxacin is expected to occur by different reaction processes in the presence of UV light and it is almost negligible in the darkness. The levofloxacin oxidation can occur from direct or indirect photolysis, through oxidizing species formed with the incidence of UV light in the catalyst and/or oxidizing species formed from the chloride ions present in the solution. In addition, the degradation efficiency can also be explained by electrostatic interactions between the electrode surface and the molecule at the different studied pHs. UV light can photoactivate the Ti/MMO/ZnO anode surface leading to the formation of the e^-/h^+ pair, that is capable of directly oxidizing LFX. In addition, its degradation can occur by anions of superoxide radicals ($O_2^{\bullet}$), hydroxyl radicals ($HO^{\bullet}$) and hydroperoxyl radicals ($HOO^{\bullet}$) produced by the photo-generated charges[42]. In addition, the incidence of UV light in a chloride solution can lead to the formation of species of active chlorine (Cl_2, HOCl and OCl^-) with high oxidizing power. These species can be transformed into other radicalary species. Thus, the UV photolysis of chlorine leads to the formation of primary $HO^{\bullet}$ and $Cl^{\bullet}$ radicals (eq 11) and secondary radical species, such as $Cl_2^{\bullet-}$ and $ClO^{\bullet}$ according to eqs 12-16 [43].

$$HOCl/OCl^- + hv(UV) \rightarrow HO^{\bullet}/O^{\bullet-} + Cl^{\bullet} \quad (11)$$

346 $Cl^{\bullet} + Cl^{-} \rightleftharpoons Cl_2^{\bullet-}$ (12)

347 $HO^{\bullet} + HOCl \rightarrow ClO^{\bullet} + H_2O$ (13)

348 $HO^{\bullet} + OCl^{-} \rightarrow ClO^{\bullet} + OH^{-}$ (14)

349 $Cl^{\bullet} + HOCl \rightarrow ClO^{\bullet} + H^{+} + Cl^{-}$ (15)

350 $Cl^{\bullet} + OCl^{-} \rightarrow ClO^{\bullet} + Cl^{-}$ (16)

351 $HO^{\bullet}$ is a strong non-selective oxidant, while reactive chlorine species (RCS)
352 such as $Cl^{\bullet}$, $Cl_2^{\bullet-}$ and $ClO^{\bullet}$ are selective [44]. $Cl^{\bullet}$ in addition to being selective, it has
353 greater reactivity than $HO^{\bullet}$ in certain organic compounds. $Cl_2^{\bullet-}$ for example, is selective
354 for olefinic compounds and aromatic rings substituted with hydroxy, methoxy and
355 amino groups while $ClO^{\bullet}$ is selective for aromatic compounds with methoxy groups
356 [43,45]. Due to the selectivity of RCS for different structures of organic compounds, the
357 UV/chlorine process can complement the degradation of these compounds, which
358 sometimes does not happen with $HO^{\bullet}$.

359 The relative concentration of a particular reactive chlorine species is strongly
360 dependent on the pH of the solution. At medium to low pH (3-7), the main species is
361 HOCl [46]. In this pH range, the highest levels of levofloxacin mineralization were
362 observed in both photolysis and photoelectrolysis (Figure 3) and which can be
363 associated to the enhanced formation of radicals by reactions 11, 13 and 15. Thus, the
364 radicals produced from the HOCl homolysis with the incidence of UVC light may have
365 contributed to the mineralization of the molecule. At basic pH, the main species is OCl^{-},
366 Figure 4 [47]. The highest degradation rates were observed at pH 9; however, at this pH,
367 there was a decrease in the mineralization rate of levofloxacin. In addition to the
368 presence of the reactive OCl^{-} species, the formation of $HO^{\bullet}$ at basic pH is also
369 facilitated. The high concentration of radicals in this medium may have led to the rapid

degradation of levofloxacin. On the other hand, the mineralization of molecule may have been affected by parallel reactions, such as recombination of oxidizing species due to its high concentration and reactivity and the formation of oxidants byproducts such as chlorates[37,48].

Figure 8 shows the inorganic ionic species (Cl^-, ClO_3^-, NH_4^+, NO_3^-) formed during the photolysis, electrolysis and photoelectrolysis of LFX. A slight variation in the concentration of Cl^- species was observed over time for all the studied processes. There was the formation of the unwanted dangerous species ClO_3^-, especially important at alkaline pHs, which is consistent with the speciation of chlorine discussed previously (Figure 8a), pointing out the role of the chlorine radicalary species on the mineralization at acidic pHs and the inactivation of these species at alkaline pHs after evolving to chlorates. The formation of ClO_4^- was not observed in the investigated processes.

During the mineralization of LFX, nitrogen is expected to be released. According to the literature, it should be transformed into NH_4^+, NO_2^- and/or NO_3^- ions [49]. Figure 8b shows the concentrations of NH_4^+ and NO_3^- released during electrolysis, photolysis and photoelectrolysis, respectively. The NO_2^- ions were not detected under the studied conditions and this can be explained because due to its high instability in oxidizing medium, NO_2^- can be quickly oxidized and therefore it is difficult to be detected. The NH_4^+ ion was formed only in an acid medium during photolysis. However, the dominant species of inorganic nitrogen formed during the degradation of LFX at different pHs was NO_3^-, with the highest concentrations found in acidic pH (2.4 mg L^{-1}) and neutral (1.6 mg L^{-1}) for photoelectrolysis. Previous works demonstrate that formation of nitrates during the oxidation of organics containing nitrogen has been the preferred pathway in electrochemical processes [50–52].

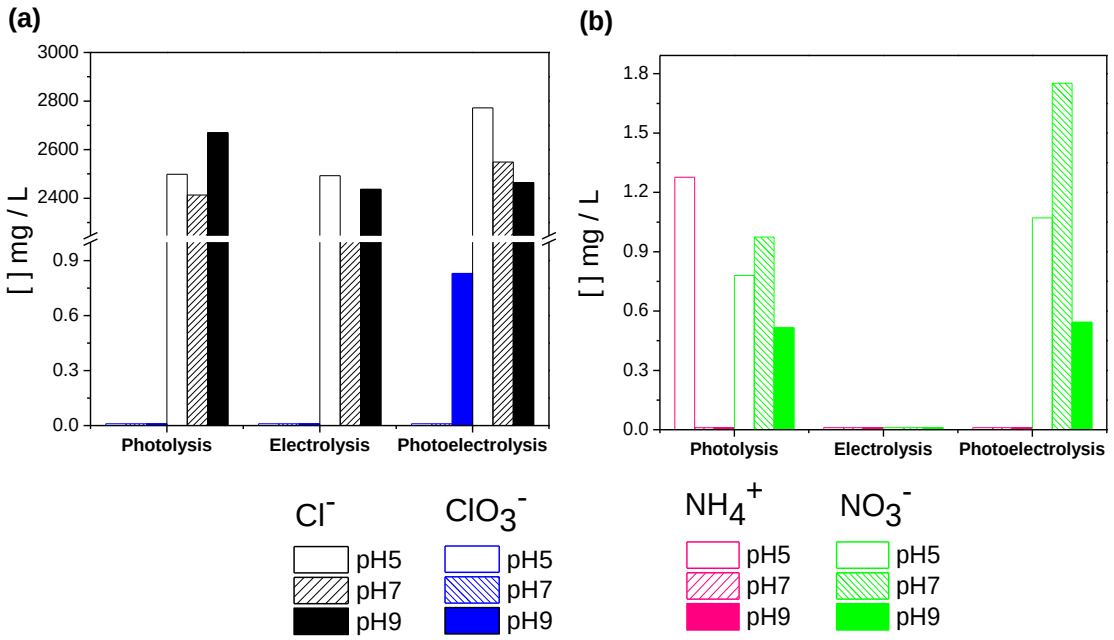

Figure 8. Inorganic ions such as Cl^- and ClO_3^- (a) and NH_4^+ and NO_3^- (b) formed at photolysis, electrolysis (0.2 V) and photo-electrolysis (0.2 V and UV) of 20 ppm levofloxacin with Ti/MMO/ZnO in 0.1 mol L^{-1} NaCl at pH 5.0, pH 7.0 and pH 9.0.

Finally, Figure 9 shows an oxidation conceptual model for LFX in wastes containing large amounts of chloride ions, ultraviolet light and Ti/MMO/ZnO as a photoanode. One can observe the different processes responsible for the degradation of LFX, such as direct and indirect photolysis, activation of oxidizing radicals by polarization and/or incidence of UV light forming reactive species of chlorine, hydroxyl and superoxide radicals, in addition to the electron/hole pair in the Ti/MMO/ZnO catalyst with high oxidizing power.

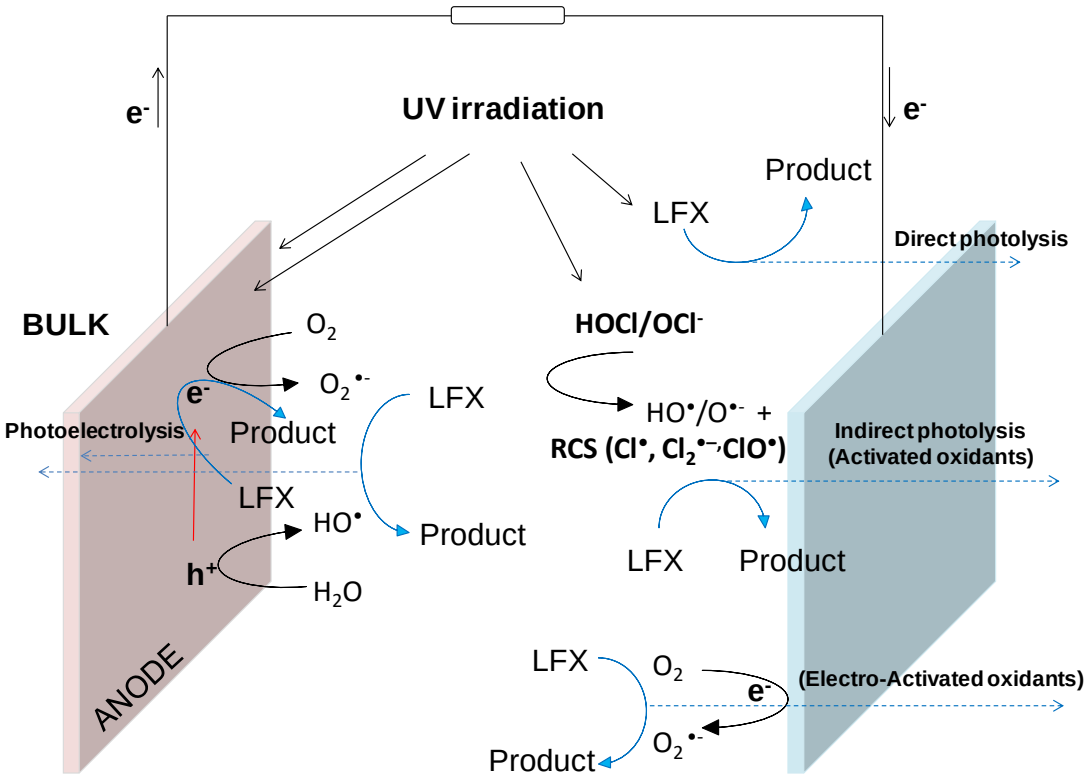

406

407 **Figure 9.** Model of the photoelectro-oxidation of LFX in wastes containing large

408 amounts of chloride ions using Ti/MMO/ZnO such as photoanode.

409

410 **Conclusions**

411 From this work, the following conclusions can be drawn:

412 - LFX can be treated by photolysis and photoelectrolysis but not by direct
413 electrolysis using Ti/MMO/ZnO anodes. Degradation efficiency was dependent
414 on the pH of the solution, the oxidizing species formed and the photoactivation
415 of Ti/MMO/ZnO.
416 - The highest rates of degradation and formation of organic intermediates were
417 obtained at basic pH in photolysis and photoelectrolysis experiments. However,
418 the mineralization of LFX was promoted at acidic pHs. This can be related to the
419 formation of certain oxidizing species at these pHs and to the acid-base
420 equilibrium of LFX to form anionic, cationic and dipolar species that facilitate
421 or hinder their degradation.

- The high concentration of hydroxyl radicals combined with reactive chlorine species formed at basic pH may have reduced the efficiency of the degradation process, due to the recombination reactions of these species.
- The highest kinetics were found in the experiments with light irradiation. Photoelectrolysis was more efficient in the degradation and mineralization of levofloxacin when compared to electrolysis and photolysis in NaCl medium, showing the synergistic effect between the photoactivation of Ti/MMO/ZnO by UVC light and the applied potential. In addition, it was observed a higher formation of inorganic ions such as NH_4^+ and NO_3^-, characteristic of LFX mineralization during photoelectrolysis, showing greater fragmentation of the molecule.
- Although the formation of ClO_3^- ions was detected, these ions were formed in basic medium and in very low concentrations during photoelectrolysis with Ti/MMO/ZnO. This indicates that it is possible to use this electrode in acidic and neutral conditions in a chloride environment in the efficient degradation of refractory pollutants without the formation of dangerous chlorine species.

Acknowledgements

Financial support from the Spanish Agencia Estatal de Investigación through project PID2019-110904RB-I00, and Junta de Comunidades de Castilla-La Mancha (JCCM) through the project SBPLY/17/180501/000396, is gratefully acknowledged. Financial support by Brazilian research funding agencies is gratefully acknowledged: CNPq (grants no 465571/2014-0, 302874/2017-8, 301492/2013-1 and 427452/2018-0); FAPESP (grants #2014/50945-4, #2016/08760-2, #2019/04084-0 and #2017/10118-0) and CAPES-Finance Code 001.

References

[1] L. Zhao, J. Deng, P. Sun, J. Liu, Y. Ji, N. Nakada, Z. Qiao, H. Tanaka, Y. Yang, Nanomaterials for treating emerging contaminants in water by adsorption and photocatalysis: Systematic review and bibliometric analysis, Sci. Total Environ. 627 (2018) 1253–1263. doi:10.1016/j.scitotenv.2018.02.006.

[2] D. Fabbri, M.J. López-Muñoz, A. Daniele, C. Medana, P. Calza, Photocatalytic abatement of emerging pollutants in pure water and wastewater effluent by TiO2 and Ce-ZnO: Degradation kinetics and assessment of transformation products, Photochem. Photobiol. Sci. 18 (2019) 845–852. doi:10.1039/c8pp00311d.

[3] L.A. Goulart, S.A. Alves, L.H. Mascaro, Photoelectrochemical degradation of bisphenol A using Cu doped WO 3 electrodes, J. Electroanal. Chem. 839 (2019) 123–133. doi:10.1016/j.jelechem.2019.03.027.

[4] D. Nasuhoglu, A. Rodayan, D. Berk, V. Yargeau, Removal of the antibiotic levofloxacin (LEVO) in water by ozonation and TiO 2 photocatalysis, Chem. Eng. J. 189–190 (2012) 41–48. doi:10.1016/j.cej.2012.02.016.

[5] R.S. Rocha, R.B. Valim, L.C. Trevelin, F.L. Silva, J.R. Steter, M. Zaiat, M.R.V. Lanza, New operational mode of an electrochemical reactor and its application to the degradation of levofloxacin, J. Environ. Chem. Eng. 5 (2017) 4441–4446. doi:10.1016/j.jece.2017.08.041.

[6] M.E. Mahmoud, A.M. El-Ghanam, R.H.A. Mohamed, S.R. Saad, Enhanced adsorption of Levofloxacin and Ceftriaxone antibiotics from water by assembled composite of nanotitanium oxide/chitosan/nano-bentonite, Mater. Sci. Eng. C. 108 (2020) 110199. doi:10.1016/j.msec.2019.110199.

[7] S. Oros-Ruiz, R. Zanella, B. Prado, Photocatalytic degradation of trimethoprim by metallic nanoparticles supported on TiO2-P25, J. Hazard. Mater. 263 (2013) 28–35. doi:10.1016/j.jhazmat.2013.04.010.

[8] Q. Chen, Y. Xin, X. Zhu, Au-Pd nanoparticles-decorated TiO2 nanobelts for photocatalytic degradation of antibiotic levofloxacin in aqueous solution, Electrochim. Acta. 186 (2015) 34–42. doi:10.1016/j.electacta.2015.10.095.

[9] G. Gupta, A. Kaur, A.S.K. Sinha, S.K. Kansal, Photocatalytic degradation of levofloxacin in aqueous phase using Ag/AgBr/BiOBr microplates under visible light, Mater. Res. Bull. 88 (2017) 148–155. doi:10.1016/j.materresbull.2016.12.016.

[10] Z.L. Bai, Q. Chen, S.D. Yang, F. Zhang, H.Y. Wang, D.L. Yang, W.Y. Ding, Toxic effects of levofloxacin on rat annulus fibrosus cells: An in-vitro study, Med. Sci. Monit. 20 (2014) 2205–2212. doi:10.12659/MSM.892610.

[11] A. Orzoł, A.I. Piotrowicz-Cieślak, Levofloxacin is phytotoxic and modifies the protein profile of lupin seedlings, Environ. Sci. Pollut. Res. 24 (2017) 22226–22240. doi:10.1007/s11356-017-9845-0.

[12] G. Lu, Z. Lun, H. Liang, H. Wang, Z. Li, W. Ma, In situ fabrication of BiVO4-CeVO4 heterojunction for excellent visible light photocatalytic degradation of levofloxacin, J. Alloys Compd. 772 (2019) 122–131. doi:10.1016/j.jallcom.2018.09.064.

[13] W. Guo, Y. Shi, H. Wang, H. Yang, G. Zhang, Intensification of sonochemical degradation of antibiotics levofloxacin using carbon tetrachloride, Ultrason. Sonochem. 17 (2010) 680–684. doi:10.1016/j.ultsonch.2010.01.004.

[14] K.H. Wammer, A.R. Korte, R.A. Lundeen, J.E. Sundberg, K. McNeill, W.A. Arnold, Direct photochemistry of three fluoroquinolone antibacterials:

Norfloxacin, ofloxacin, and enrofloxacin, Water Res. 47 (2013) 439–448. doi:10.1016/j.watres.2012.10.025.

[15] J.M. Aquino, D.W. Miwa, M.A. Rodrigo, A.J. Motheo, Treatment of actual effluents produced in the manufacturing of atrazine by a photo-electrolytic process, Chemosphere. 172 (2017) 185–192. doi:10.1016/j.chemosphere.2016.12.154.

[16] E. Brillas, A review on the degradation of organic pollutants in waters by UV photoelectro-fenton and solar photoelectro-fenton, J. Braz. Chem. Soc. 25 (2014) 393–417. doi:10.5935/0103-5053.20130257.

[17] X. Xu, L. Hu, N. Gao, S. Liu, S. Wageh, A.A. Al-Ghamdi, A. Alshahrie, X. Fang, Controlled growth from ZnS nanoparticles to ZnS-CdS nanoparticle hybrids with enhanced photoactivity, Adv. Funct. Mater. 25 (2015) 445–454. doi:10.1002/adfm.201403065.

[18] J. Diaz-Angulo, J. Porras, M. Mueses, R.A. Torres-Palma, A. Hernandez-Ramirez, F. Machuca-Martinez, Coupling of heterogeneous photocatalysis and photosensitized oxidation for diclofenac degradation: role of the oxidant species, J. Photochem. Photobiol. A Chem. 383 (2019) 112015. doi:10.1016/j.jphotochem.2019.112015.

[19] P. Fageria, S. Gangopadhyay, S. Pande, Synthesis of ZnO/Au and ZnO/Ag nanoparticles and their photocatalytic application using UV and visible light, RSC Adv. 4 (2014) 24962–24972. doi:10.1039/c4ra03158j.

[20] S. Zhu, D. Wang, Photocatalysis: Basic principles, diverse forms of implementations and emerging scientific opportunities, Adv. Energy Mater. 7 (2017) 1–24. doi:10.1002/aenm.201700841.

[21] H. Fu, T. Xu, S. Zhu, Y. Zhu, Photocorrosion inhibition and enhancement of photocatalytic activity for ZnO via hybridization with C60, Environ. Sci. Technol. 42 (2008) 8064–8069. doi:10.1021/es801484x.

[22] B. Subash, B. Krishnakumar, M. Swaminathan, M. Shanthi, Highly efficient , solar active and reusable photocatalyst , Zr loaded Ag-ZnO for Reactive Red 120 dye degradation with synergistic effect and dye sensitized mechanism Highly efficient , solar active and reusable photocatalyst , Zr loaded Ag-ZnO for React, (2012). doi:10.1021/la303842c.

[23] H. Zhang, R. Zong, Y. Zhu, Photocorrosion inhibition and photoactivity enhancement for zinc oxide via hybridization with monolayer polyaniline, J. Phys. Chem. C. 113 (2009) 4605–4611. doi:10.1021/jp810748u.

[24] V. Cristino, G. Longobucco, N. Marchetti, S. Caramori, C.A. Bignozzi, A. Martucci, A. Molinari, R. Boaretto, C. Stevanin, R. Argazzi, M. Dal Colle, R. Bertoncello, L. Pasti, Photoelectrochemical degradation of pharmaceuticals at β25 modified WO3 interfaces, Catal. Today. 340 (2020) 302–310. doi:10.1016/j.cattod.2018.09.020.

[25] V. Cristino, L. Pasti, N. Marchetti, S. Berardi, C.A. Bignozzi, A. Molinari, F. Passabi, S. Caramori, L. Amidani, M. Orlandi, N. Bazzanella, A. Piccioni, J. Kopula Kesavan, F. Boscherini, L. Pasquini, Photoelectrocatalytic degradation of emerging contaminants at WO3/BiVO4 photoanodes in aqueous solution,

Photochem. Photobiol. Sci. 18 (2019) 2150–2163. doi:10.1039/c9pp00043g.

[26] R. Gupta, J.M. Modak, G. Madras, Behavioral analysis of simultaneous photo-electro-catalytic degradation of antibiotic resistant: E. coli and antibiotic via ZnO/CuI: A kinetic and mechanistic study, Nanoscale Adv. 1 (2019) 3992–4008. doi:10.1039/c9na00483a.

[27] Z. Cheng, L. Ling, Z. Wu, J. Fang, P. Westerhoff, C. Shang, A novel visible-light-driven photocatalytic chlorine activation process for carbamazepine degradation in drinking water, Environ. Sci. Technol. (2020). doi:10.1021/acs.est.0c03170.

[28] T. de Mello Florêncio, K.S. de Araújo, R. Antonelli, A.L. de Toledo Fornazari, P.C.R. da Cunha, L.H. da Silva Bontempo, A. de Jesus Motheo, A.C. Granato, G.R.P. Malpass, Photo-assisted electrochemical degradation of simulated textile effluent coupled with simultaneous chlorine photolysis, Environ. Sci. Pollut. Res. 23 (2016) 19292–19301. doi:10.1007/s11356-016-6912-x.

[29] C.D.N. Brito, D.M. De Araújo, C.A. Martínez-Huitle, M.A. Rodrigo, Understanding active chlorine species production using boron doped diamond films with lower and higher sp3/sp2 ratio, Electrochem. Commun. 55 (2015) 34–38. doi:10.1016/j.elecom.2015.03.013.

[30] D.J. Soucek, T.K. Linton, C.D. Tarr, A. Dickinson, N. Wickramanayake, C.G. Delos, L.A. Cruz, Influence of water hardness and sulfate on the acute toxicity of chloride to sensitive freshwater invertebrates, Environ. Toxicol. Chem. 30 (2011) 930–938. doi:10.1002/etc.454.

[31] Y. Wang, Y. Xue, C. Zhang, Generation and application of reactive chlorine species by electrochemical process combined with UV irradiation: Synergistic mechanism for enhanced degradation performance, Sci. Total Environ. 712 (2020) 136501. doi:10.1016/j.scitotenv.2020.136501.

[32] R. de Mello, L.H.E. Santos, M.M.S. Pupo, K.I.B. Eguiluz, G.R. Salazar-Banda, A.J. Motheo, Alachlor removal performance of Ti/Ru0.3Ti0.7O2 anodes prepared from ionic liquid solution, J. Solid State Electrochem. 22 (2018) 1571–1580. doi:10.1007/s10008-017-3700-6.

[33] O. Ridge, M. Kolthoff, Volumetric Determination of Persulfate in the Presence of Organic Substances, (n.d.) 298–301.

[34] L.M. da Silva, G. de Oliveira Santiago Santos, M.M. de Salles Pupo, K.I.B. Eguiluz, G.R. Salazar-Banda, Influence of heating rate on the physical and electrochemical properties of mixed metal oxides anodes synthesized by thermal decomposition method applying an ionic liquid, J. Electroanal. Chem. 813 (2018) 127–133. doi:10.1016/j.jelechem.2018.02.026.

[35] S. Trasatti, Physical electrochemistry of ceramic oxides, Electrochim. Acta. 36 (1991) 225–241. doi:10.1016/0013-4686(91)85244-2.

[36] T. Actu, E.S.P.B. V, G.P. Vercesi, J. Rolewicz, J. Hinden, G. Branch, Characterization of dsa-tyf'e oxygen evolving electrodes. choice of base metal, 176 (1991) 31–47.

[37] G.O.S. Santos, K.I.B. Eguiluz, G.R. Salazar-Banda, C. Saez, M.A. Rodrigo,

584 Photoelectrolysis of clopyralid wastes with a novel laser-prepared MMO-
585 RuO2TiO2 anode, Chemosphere. 244 (2020) 125455.
586 doi:10.1016/j.chemosphere.2019.125455.

587 [38] X. Qin, F. Liu, G. Wang, L. Weng, L. Li, Adsorption of levofloxacin onto
588 goethite: Effects of pH, calcium and phosphate, Colloids Surfaces B
589 Biointerfaces. 116 (2014) 591–596. doi:10.1016/j.colsurfb.2013.09.056.

590 [39] I. Ahmad, R. Bano, M.A. Sheraz, S. Ahmed, T. Mirza, S.A. Ansari,
591 Photodegradation of levofloxacin in aqueous and organic solvents: A kinetic
592 study, Acta Pharm. 63 (2013) 223–229. doi:10.2478/acph-2013-0011.

593 [40] M.S. Gudaganatti, M.S. Hanagadakar, Transformation of levofloxacin during
594 water chlorination process : kinetics and pathways, 37 (2012) 366–382.
595 doi:10.3184/146867812X13440034591571.

596 [41] J. Llanos, I. Moraleda, C. Sáez, M.A. Rodrigo, P. Cañizares, Electrochemical
597 production of perchlorate as an alternative for the valorization of brines,
598 Chemosphere. 220 (2019) 637–643. doi:10.1016/j.chemosphere.2018.12.153.

599 [42] M. Stan, A. Popa, D. Toloman, A. Dehelean, I. Lung, G. Katona, Enhanced
600 photocatalytic degradation properties of zinc oxide nanoparticles synthesized by
601 using plant extracts, Mater. Sci. Semicond. Process. 39 (2015) 23–29.
602 doi:10.1016/j.mssp.2015.04.038.

603 [43] K. Guo, Z. Wu, C. Shang, B. Yao, S. Hou, X. Yang, W. Song, J. Fang, Radical
604 Chemistry and Structural Relationships of PPCP Degradation by UV/Chlorine
605 Treatment in Simulated Drinking Water, Environ. Sci. Technol. 51 (2017)
606 10431–10439. doi:10.1021/acs.est.7b02059.

607 [44] J. Fang, Y. Fu, C. Shang, The roles of reactive species in micropollutant
608 degradation in the UV/free chlorine system, Environ. Sci. Technol. 48 (2014)
609 1859–1868. doi:10.1021/es4036094.

610 [45] Z.B. Alfassi, R.E. Huie, S. Mosseri, P. Neta, Kinetics of one-electron oxidation
611 by the ClO radical, Int. J. Radiat. Appl. Instrumentation. Part. 32 (1988) 85–88.
612 doi:10.1016/1359-0197(88)90018-5.

613 [46] I. Sánchez-Montes, N. Wachter, B.F. Silva, J.M. Aquino, Comparison of UVC-
614 based advanced oxidation processes in the mineralization of bisphenol A:
615 Identification of oxidation by products and toxicity evaluation, Chem. Eng. J. 386
616 (2020) 123986. doi:10.1016/j.cej.2019.123986.

617 [47] Y. Feng, D.W. Smith, J.R. Bolton, Photolysis of aqueous free chlorine species
618 (HOCl and OCl-) with 254 nm ultraviolet light, J. Environ. Eng. Sci. 6 (2007)
619 277–284. doi:10.1139/S06-052.

620 [48] D.M. De Araújo, S. Cotillas, C. Sáez, P. Cañizares, C.A. Martínez-Huitle, M.A.
621 Rodrigo, Activation by light irradiation of oxidants electrochemically generated
622 during Rhodamine B elimination, J. Electroanal. Chem. 757 (2015) 144–149.
623 doi:10.1016/j.jelechem.2015.09.025.

624 [49] Y. Gong, J. Li, Y. Zhang, M. Zhang, X. Tian, A. Wang, Partial degradation of
625 levofloxacin for biodegradability improvement by electro-Fenton process using
626 an activated carbon fiber felt cathode, J. Hazard. Mater. 304 (2016) 320–328.

doi:10.1016/j.jhazmat.2015.10.064.

[50] M.J. Martin De Vidales, M. Millán, C. Sáez, P. Cañizares, M.A. Rodrigo, What happens to inorganic nitrogen species during conductive diamond electrochemical oxidation of real wastewater?, Electrochem. Commun. 67 (2016) 65–68. doi:10.1016/j.elecom.2016.03.014.

[51] E. Lacasa, P. Cañizares, J. Llanos, M.A. Rodrigo, Removal of nitrates by electrolysis in non-chloride media: Effect of the anode material, Sep. Purif. Technol. 80 (2011) 592–599. doi:10.1016/j.seppur.2011.06.015.

[52] L. Oliviero, J. Barbier, D. Duprez, Wet air oxidation of nitrogen-containing organic compounds and ammonia in aqueous media, Appl. Catal. B Environ. 40 (2003) 163–184. doi:10.1016/S0926-3373(02)00158-3.